ResearchGate

See discussions, stats, and author profiles for this publication at: https://www.researchgate.net/publication/278075479

Hysteresis Analysis Based on the Ferroelectric Effect in Hybrid Perovskite Solar Cells

ARTICLE *in* JOURNAL OF PHYSICAL CHEMISTRY LETTERS · NOVEMBER 2014

Impact Factor: 7.46 · DOI: 10.1021/jz502111u

CITATIONS
44

READS
35

8 AUTHORS, INCLUDING:

Zhao Yicheng
Peking University
3 PUBLICATIONS **43** CITATIONS
SEE PROFILE

Heng Li
Peking University
12 PUBLICATIONS **158** CITATIONS
SEE PROFILE

Qing Zhao
Peking University
174 PUBLICATIONS **3,646** CITATIONS
SEE PROFILE

Available from: Heng Li
Retrieved on: 30 January 2016

THE JOURNAL OF PHYSICAL CHEMISTRY Letters

Letter

pubs.acs.org/JPCL

Hysteresis Analysis Based on the Ferroelectric Effect in Hybrid Perovskite Solar Cells

Jing Wei,[†,⊥] Yicheng Zhao,[†,⊥] Heng Li,[†] Guobao Li,[§] Jinlong Pan,[§] Dongsheng Xu,[§] Qing Zhao,*[,†,‡] and Dapeng Yu*[,†,‡]

[†]State Key Laboratory for Mesoscopic Physics, School of Physics and [§]College of Chemistry and Molecular Engineering, Peking University, Beijing 100871, People's Republic of China

[‡]Collaborative Innovation Center of Quantum Matter, 100084 Beijing, China

Supporting Information

ABSTRACT: The power conversion efficiency (PCE) of $CH_3NH_3PbX_3$ (X = I, Br, Cl) perovskite solar cells has been developed rapidly from 6.5 to 18% within 3 years. However, the anomalous hysteresis found in $I-V$ measurements can cause an inaccurate estimation of the efficiency. We attribute the phenomena to the ferroelectric effect and build a model based on the ferroelectric diode to explain it. The ferroelectric effect of $CH_3NH_3PbI_{3-x}Cl_x$ is strongly suggested by characterization methods and the $E-P$ (electrical field−polarization) loop. The hysteresis in $I-V$ curves is found to greatly depend on the scan range as well as the velocity, which is well explained by the ferroelectric diode model. We also find that the current signals show exponential decay in ∼10 s under prolonged stepwise measurements, and the anomalous hysteresis disappears using these stabilized current values. The experimental results accord well with the model based on ferroelectric properties and prove that prolonged stepwise measurement is an effective way to evaluate the real efficiency of perovskite solar cells. Most importantly, this work provides a meaningful perspective that the ferroelectric effect (if it really exists) should be paid special attention in the optimization of perovskite solar cells.

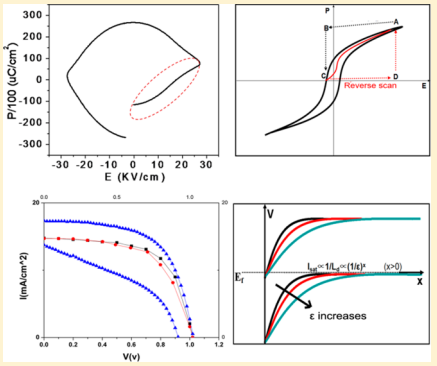

SECTION: Energy Conversion and Storage; Energy and Charge Transport

Perovskite solar cells have rapidly risen to the forefront of emerging photovoltaic applications, demonstrating rapidly rising efficiencies with the latest reported efficiency up to 19.3%.[1] Until recently, perovskite solar cells have developed into three main architectures, (1) perovskite material used as sensitizer coating on TiO_2 nanoparticles,[2,3] (2) a mesoporous TiO_2 layer immersed in perovskite material with a capping layer on the top,[4] (3) planar heterojunction solar cells without a TiO_2 scaffold,[5] all of which can get a high efficiency. However, most perovskite solar cells have the hysteresis problem in $I-V$ curves reported by many groups.[4,6−9] Anomalous hysteresis results in a puzzle of the real conversion efficiency, and possibly the large discrepancy between the forward scan and reverse scan can induce a considerable error in evaluating the real cell efficiency (nomenclature: reverse scan is called when measuring from large to small voltage, and contrarily, forward scan is called when measuring from small to large voltage). Identifying the physical mechanism of the effect and clarifying its implications on cell efficiency are extremely important in future research directions.

The hysteresis phenomenon had been reported by Snaith et al., and three possible causes were proposed.[7] Park et al. described the hysteresis effects in terms of perovskite size and the presence or absence of a mesoporous TiO_2 layer.[9] Walsh et al. proposed that the internal electrical fields associated with polarization domains contribute to hysteresis in the current−voltage response of hybrid perovskite solar cells.[10] However, their explanation on the relation between the ferroelectric effect and $I-V$ curves is not comprehensive. Moreover, there is no experimental evidence in this report. Very recently, Seok et al. obtained an efficiency of 16.2% without hysteresis in a so-called "bilayered cell" using solvent engineering.[4] They suggested that the large diffusion capacitance of such cells may contribute to this phenomenon. So far, many groups pointed out the hysteresis phenomenon, but systematic investigation on the reason and the underlying working principle for the hysteresis has been rarely conducted. Because the anomalous hysteresis is a central challenge for adoption of perovskite photovoltaics, understanding and resolving the hysteresis is essential for future progress of perovskite solar cells.

In this Letter, the hysteresis in $I-V$ curves is attributed to the ferroelectric effect in perovskite material, and ferroelectric domains are strongly suggested by common characterization methods in the ferroelectric material field. On the basis of this special effect, we build a ferroelectric diode model to explain

Received: October 4, 2014
Accepted: October 24, 2014

 © XXXX American Chemical Society dx.doi.org/10.1021/jz502111u | J. Phys. Chem. Lett. 2014, 5, 3937−3945

the anomalous hysteresis phenomena. We use long-stepwise measurement to exclude the influence of the slow process caused by the ferroelectric effect and find that $I-V$ curves extracted from long-stepwise measurement show hysteresis-free behavior. The obtained efficiency is believed to be the real efficiency in perovskite solar cells, which is overestimated in reverse scan and underestimated in forward scan under 0.25 V/s. The hysteresis is also found to be strongly dependent on the scan range and scan rate. The observations above can be understood comprehensively based on the ferroelectric diode model. We systematically design four types of architectures and find the continual decrease of the area in hysteresis from the planar heteojunction to sensitization. We attribute it to the different time scale of domain wall motion with different grain size in ferroelectric materials. The ferroelectric effects have a huge impact on the performance of hybrid perovskite solar cells, which needs to be carefully considered in the optimization of perovskite solar cells.

It is well-known that a number of perovskite structure materials, such as $PbTiO_3$ and $PbZrO_3$, are ferroelectric materials.[11,12] $CH_3NH_3PbX_3$ (X = I, Br, Cl) is also expected to contain ferroelectric domains, and the relationship with hysteresis has been proposed by many works in hybrid perovskite solar cells. However, until recently, little experimental evidence has been reported, as well as specific analysis on the relation between ferroelectric properties and $I-V$ hysteresis.

Usually, to confirm the existence of the ferroelectric effect, one should first test if this material is included in the 10 ferroelectric material point groups by X-ray diffraction (XRD) data. To further prove the acentrosymmetric structure of the material,[13−15] Raman and Fourier transform infrared spectroscopy (FTIR) spectra can be used if the vibrational mode coexists because the activities in Raman and IR spectroscopy are mutually exclusive in a crystal with inversion symmetry.[16] Finally, the ferroelectric domain structure can be confirmed by $E-P$ (electric field−polarization) measurement or piezoelectric force microscopy (PFM).

The XRD of a solution-processed $CH_3NH_3PbI_{3-x}Cl_x$ thin film (Figure S1 in the Supporting Information) demonstrates an *I4cm* crystal structure at room temperature (β-phase), which has a lower symmetry compared to *P4mm* (α-phase).[17,18] The primitive cell in the tetragonal structure presents an anisotropic crystal field. Raman spectra (Figure 1a) show peaks at about 65, 120, and 180 cm^{-1}, which can be assigned to the Pb−I vibrational mode, MA^+ vibrational mode, and MA^+ torsional mode, respectively.[19,20] The peaks at 65 and 180 cm^{-1} are matched up to the ones in FTIR spectra (Figure 1b), which indicates that the crystal structure has no inversion symmetry. Considering that MA^+ cations might be disordered around the eight possible orientations inside of the cube, there might exist ferroelectric domains due to the intrinsic dipole moment of MA^+ in this crystal.[8] The observations above strongly suggest that $CH_3NH_3PbX_3$ (X = I, Br, Cl) is a ferroelectric material.[21,22]

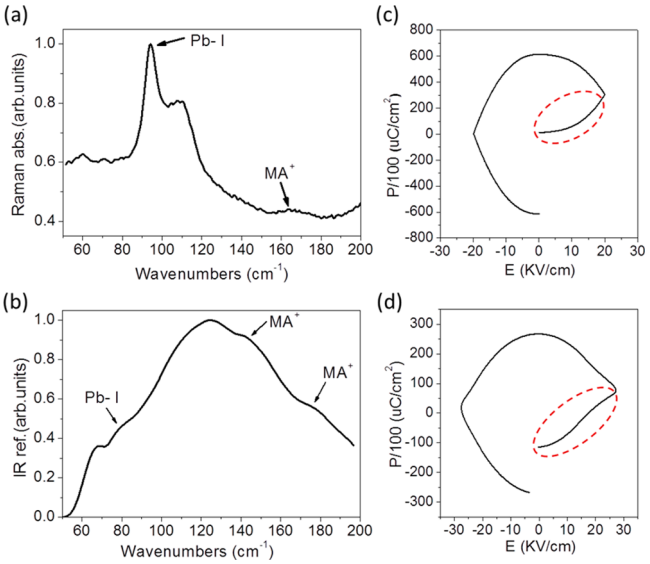

Figure 1. Ferroelectric effect measurement of $(CH_3NH_3)PbI_{3-x}Cl_x$. (a) Raman spectra, (b) FTIR spectra, (c,d) $E-P$ measurement plot of Al_2O_3 only as a control device (c) and Al_2O_3 on perovskite (d). The device architecture for $E-P$ measurement is shown in Figure S2 (Supporting Information).

$E-P$ loop measurements were applied to two samples, a hybrid perovskite film coated by Al_2O_3 films and an Al_2O_3 film without perovskite as the control device. The Al_2O_3 coating on the perovskite film was used as series capacitance to enhance the potential ferroelectric signals. Au electrodes were deposited on both faces of the samples, as shown in Figure S2 in the Supporting Information. The $E-P$ loop measures the charge quantity as a function of the bias voltage, as shown in the formula below[13]

$$Q_T = \begin{cases} cV + \dfrac{V^2}{2RA} + Q_F \approx cV + \dfrac{V^2}{2R}\dfrac{\Delta t}{|\Delta V|} + Q_F & (-V_{max} \rightarrow V_{max}) \\ cV + \dfrac{V_{max}^2}{RA} - \dfrac{V^2}{2RA} + Q_F \approx cV + \left(\dfrac{V_{max}^2}{R} - \dfrac{V^2}{2RA}\right)\dfrac{\Delta t}{|\Delta V|} + Q_F & (V_{max} \rightarrow -V_{max}) \end{cases}$$

where c is the capacitance of the dielectric layer, V is the bias voltage, Q_F, caused by ferroelectric effect, is the polarized charge quantity nonlinear to V, R is the resistance of the conductive layer, $\Delta V/\Delta t$ is the scan velocity of V, A is the scan speed of voltage, and Q_T is the total charge quantity. Here, Q_F can be expressed as P, where P stands for the polarization intensity of the hybrid perovskite material per area. If Q_F is negligible, the Q_T-E curve will be parabolic; otherwise, the Q_T-E curve will be distorted because of the nonlinear term Q_F.

The $E-P$ loop of the A_2O_3 control sample (Figure 1c) shows that the Q_T-E curve is parabolic exactly in each quadrant. Figure 1d for the perovskite sample reveals that the Q_T-E curve is warped to "S" shape obviously, especially in the fourth quadrant. In summary, Raman and FTIR spectra combinrf with $E-P$ measurements suggest that the hybrid perovskite material is a ferroelectric semiconductor, although the ferroelectric effect measured by us is much smaller than traditional perovskite ferroelectrics.

dx.doi.org/10.1021/jz502111u | J. Phys. Chem. Lett. 2014, 5, 3937−3945

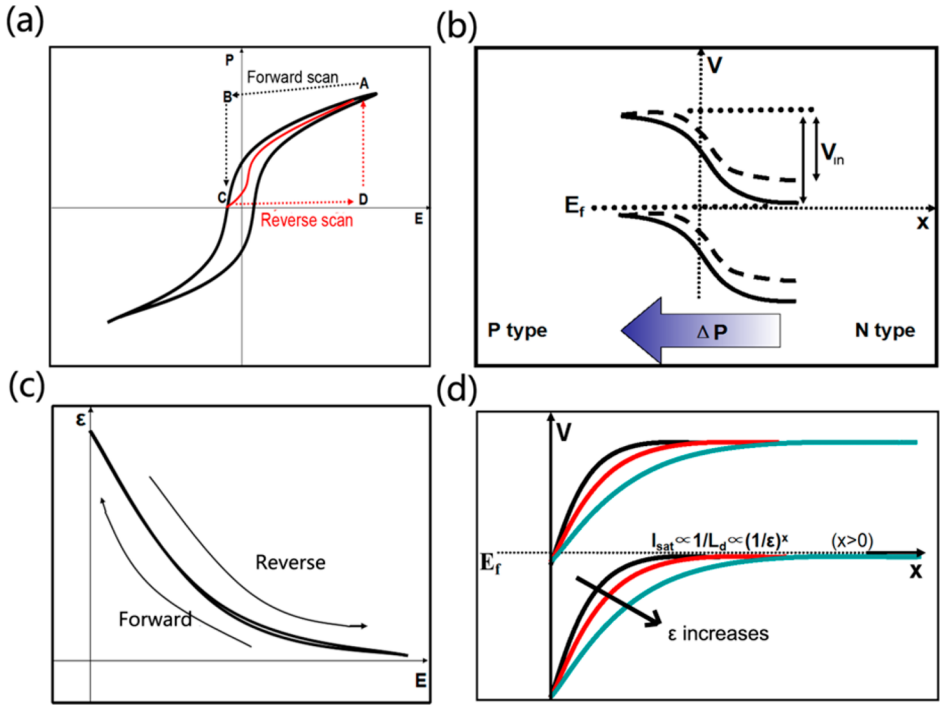

Figure 2. (a) Schematic diagram of the relationship between polarization P as a function of E in ferroelectric materials; path A−B−C indicates the forward scan under a moderate scan velocity, and path C−D−A indicates the reverse scan. (b) Schematic diagram of the energy band corrected by the excess polarization ΔP, induced by the nonrelaxed ferroelectric domain in the forward scan mode under a moderate scan velocity. The solid line reveals the energy band diagram of the p−n junction in the stable state, and the dashed line reveals the corrected one. (c) Schematic diagram of $\varepsilon(E) = dP/dE$ as a function of E in ferroelectric materials. ε between forward scan and reverse scan does not have a very large difference because ε is the slope of the function. (d) Schematic diagram of the space charge region distributed in perovskite, showing that the depletion region length is strongly dependent on ε.

Next, we are going to build up a model to analyze the relationship between the ferroelectric effect and the performance of solar cells to explain the hysteresis in $I-V$ measurements. In 1994, P. W. M. Blom built a model to explain the bistable conduction characteristic containing ferroelectric semiconducting material and claimed that the hysteresis loop of the $I-V$ plot is mainly caused by the nonlinear nature in the $E-P$ relationship.[23] Compared to common semiconductors, due to strong electron−phonon interaction, there exists a special property in ferroelectric semiconductors, the polarization-based dielectric constant (ε). The change of ε under various bias voltages affects the collection efficiency of photoinduced charge carriers.

The schematic diagram of polarization P as a function of electric field E in ferroelectrics is illustrated in Figure 2a. In the hybrid perovskite solar cells, the built-in electric field can be estimated as $E_{in} = (V_{oc} - V)/W$, where V_{oc} is the open-circuit voltage and W is the depletion region width. E_{in} equals about 10 MV/m when $V = 0$; therefore, it is expected to be a large variation of E_{in} when the bias voltage changes from −0.5 to 1.5 V. The route of ABCD marked in Figure 2a shows how P and E change when the state of the solar cell alters from short circuit to open circuit and then is returned to short circuit; the dotted line implies the transient state, which will be discussed later.

Figure 2b depicts the energy band of teh p−n junction in an excess background field ΔP. This ΔP is caused by the long relaxation time of the ferroelectric domain, and when E decreases, P needs about seconds to drop correspondingly; therefore, there exists an excess polarization field in the perovskite material, which is defined as ΔP. ΔP can be considered as a superimposed field, and the energy bands move to dotted curves correspondingly, as shown in Figure 2b. In this nonequilibrium state, the existence of ΔP causes V_{in} to decrease and consequently causes V_{oc} to decrease because V_{oc} is proportional to V_{in}. Additionally, the short-circuit current I_{sc} is mainly decided by the charge carrier diffusion length and transmission distance;[24] therefore, it can be hardly impacted by ΔP. By analyzing ΔP, we infer that it influences V_{oc} more seriously than I_{sc}.

Figure 2c shows that the permittivity $\varepsilon = dP/dE$ rises as E decreases according to the $E-P$ hysteresis loop in the first quadrant. Figure 2d shows the relationship between the depletion length based on ε in ferroelectric materials, similar to that in common semiconductors. It reveals that larger $\varepsilon(E)$ will widen the depletion region, an important factor in solar cells. Here, we give the photocurrent formula correlated with L_d

$$I = I_{sc} - I_{sat} \cdot (e^{n \cdot e \cdot (V/kT)} - 1)$$

$$I_{sat} = e \cdot n_i^2 \cdot \frac{D_n}{N_a} \cdot L_d$$

where I_{sc} is the short-circuit current, I_{sat} is the saturation current, $e = 1.6 \times 10^{-19}$C, V is the bias voltage, k is the Boltzmann constant, ε is the permittivity, T is the temperature, n_i is the intrinsic carrier concentration, D_n is the diffusion constant, L_d is the depletion length, and N_a is the concentration of acceptor states. As can be seen in the formula above, I_{sat} is negtively related to the depletion region L_d, which is dependent on $\varepsilon(E)$ in ferroelectric materials. The photocurrent is decided by I_{sat}; therefore, a larger $\varepsilon(E)$ will induce a larger photocurrent value, as well as V_{oc}. On the other hand, larger ε promotes both

dx.doi.org/10.1021/jz502111u | J. Phys. Chem. Lett. 2014, 5, 3937−3945

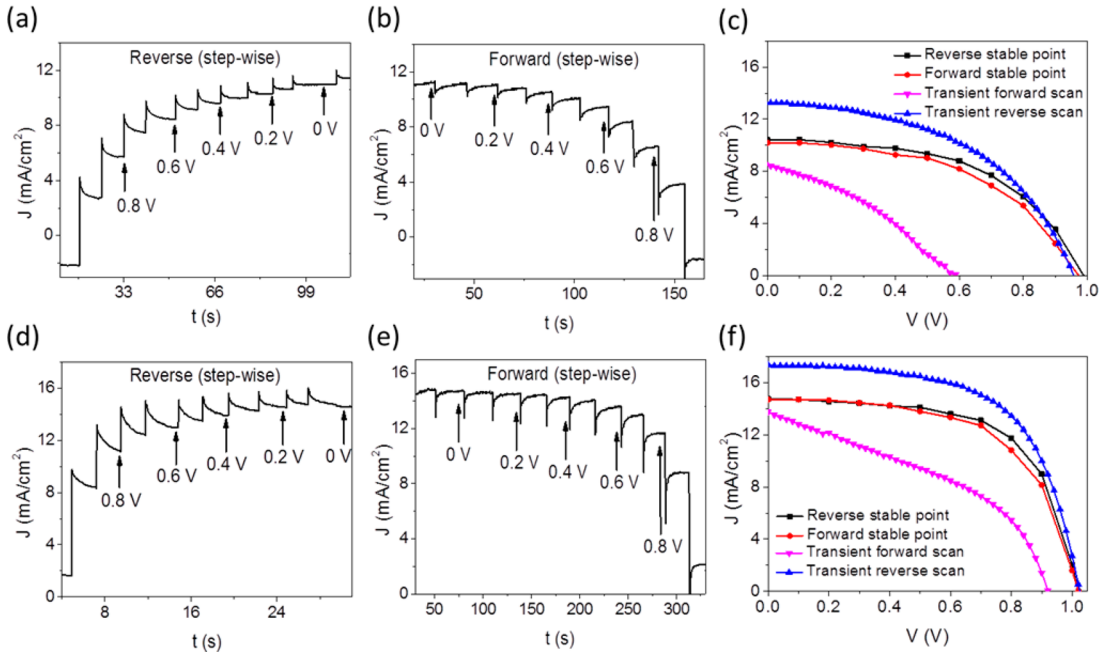

Figure 3. Long-stepwise $I-V$ measurement of perovskite solar cells. (a,b) Reverse and forward stepwise scan measurement (with a dwell time of ∼10 s per 100 mV step) for device 1. (c) Current−voltage measurement of the stable-state scan (points extracted from the point where the arrows indicate in (a,b)) and transient scan (scan velocity: 250 mV/s) in forward and reverse scans. (d,e) Reverse and forward stepwise scan measurements (with a dwell time of ∼10 s per 100 mV step) for device 2. (f) Current−voltage measurements of the stable-state scan and transient scan (scan velocity: 250 mV/s) in forward and reverse scans.

Wannier−Mott exciton separation and effective ionization of defects,[10] which is favorable to improve the efficiency. In a word, the solar cell efficiency becomes better with bigger ε.

The hysteresis phenomena observed by many groups under ∼0.25 V/s scan velocity can be explained according to the discussion above.[6−10] In forward scan mode, E_{in} is large at the beginning; therefore, the initial polarization state is in the vicinity of point A in Figure 2a, corresponding to a small ε (Figure 2c). Considering that the polarization cannot follow the scan velocity of 0.25 V/s, as E decreases, the $E-P$ state reaches the transient state B and then drops to the stable- state C in Figure 2a. Not only the average $\varepsilon(E)$ is smaller, but also, excess ΔP exists parallel to the E_{in}, compared to its corresponding stable state. However, in reverse scan mode, the initial state is around point C, corresponding to a large $\varepsilon(E)$, without excess ΔP. Before returning to the stable state A, the polarization will stay at state D for a while. A larger $\varepsilon(E)$ and smaller ΔP in the solar cell is more advantageous, leading to a larger photocurrent. Therefore, the efficiency in reverse scan is bigger than that in forward scan, which explains the discrepancy between two different scan directions.

To exclude the influence of the slow process caused by the ferroelectric effect and to discern more details of the photocurrent from the transient to stable state in perovskite solar cells, we use long-stepwise measurement to estimate the real efficiency of the solar cells. Figure 3a,b,d,e shows the long-stepwise $I-V$ measurements in reverse and forward modes for two devices that contain a mesoporous TiO_2 scaffold with a perovskite capping layer of different thicknesses. The long-stepwise $I-V$ curves were measured with a dwell time of ∼10 s per 100 mV step. As the bias voltage increases (forward mode), the photocurrent drops significantly at the beginning and then returns to a stable state at a larger value (Figure 3b,e). In contrast, as the bias voltage decreases (reverse mode), the photocurrent jumps up at first and then decreases to a stable-state current at a smaller value (Figure 3a,d). Figure 3c,f shows the extracted stable-state $I-V$ data (the extracted data points were indicated by arrows in panels a, b, d, and e) compared to the scanning data under 250 mV/s for the two tested devices, revealing that neither the forward scan nor the reverse scan under 250 mV/s reveals the static working state of the hybrid perovskite solar cell, giving rise to either over- or under-estimation of efficiency. Note that the extracted stable-state point matches well with one another regardless of the scan direction.

Considering that the ferroelectric domain relaxation time is around seconds,[25] the current change tendency with long delay time can be explained in detail based on the ferroelectric effect. From the aspect of $\varepsilon(E)$, under the stepwise scan in forward mode, the ferroelectric state switches slowly; therefore, the polarization reaches the equilibrium state after ∼10 s. Figure 3b,e shows the long relaxation time when the bias voltage steps into another value, and at each step, ε increases to a larger value and ΔP disappears gradually, resulting in a gradual increase of photocurrent (Figure 3b,e). In the reverse stepwise scan, when the voltage steps to a smaller value, ε decreases slowly to the stable value, causing the current value to increase sharply then decrease correspondingly. It explains why the efficiency under stable-state scan is larger than forward scan but smaller than reverse scan under 0.25 V/s. More importantly, the extracted stable-state $I-V$ curves match well regardless of the scan direction (Figure 3c,f), which can be understood by the small discrepancy of $\varepsilon(E)$ between two opposite scan directions.

On the basis of the ferroelectric effect in perovskite material, we successfully uncovered the underlying physics reason for the observed anomalous hysteresis and explain the reason why reverse scan could get a better efficiency than forward scan under 0.25 V/s. More importantly, we found that stable-state

dx.doi.org/10.1021/jz502111u | J. Phys. Chem. Lett. 2014, 5, 3937−3945

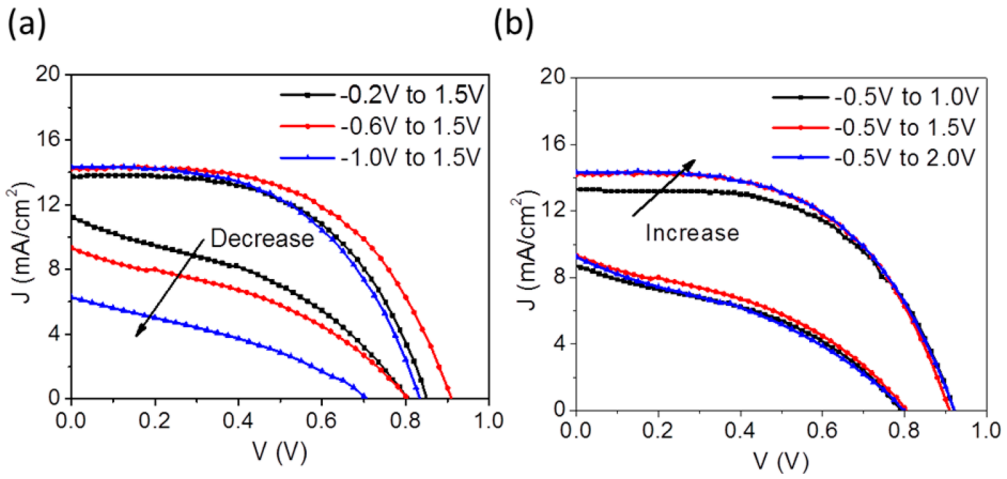

Figure 4. $I-V$ curves of perovskite solar cells under different scanning starting points in forward and reverse scan. (a) $I-V$ curves with different starting points of scanning, from −0.2 to −1 V; the efficiency decreases and the efficiency discrepancy increases from ∼2.5 to ∼7%, correspondingly. (b) $I-V$ curves with different ending points of scanning, from 1 to 2 V; the efficiency discrepancy shows no obvious variation.

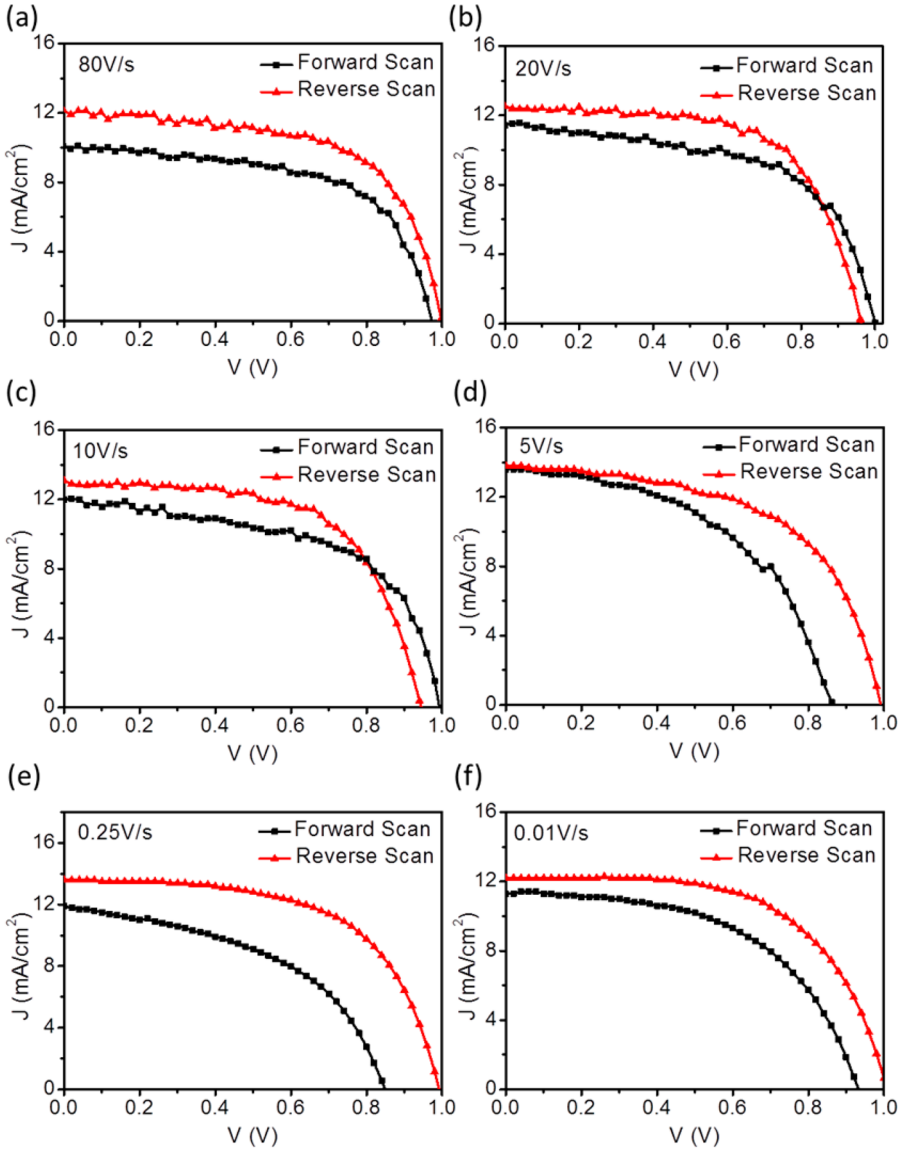

Figure 5. Current−voltage measurements of perovskite solar cells under a series of different scanning velocities from 80 to 0.01 V/s in forward and reverse scan: (a) 80, (b) 20, (c) 10, (d) 5, (e) 0.25, and (f) 0.01 V/s.

dx.doi.org/10.1021/jz502111u | J. Phys. Chem. Lett. 2014, 5, 3937−3945

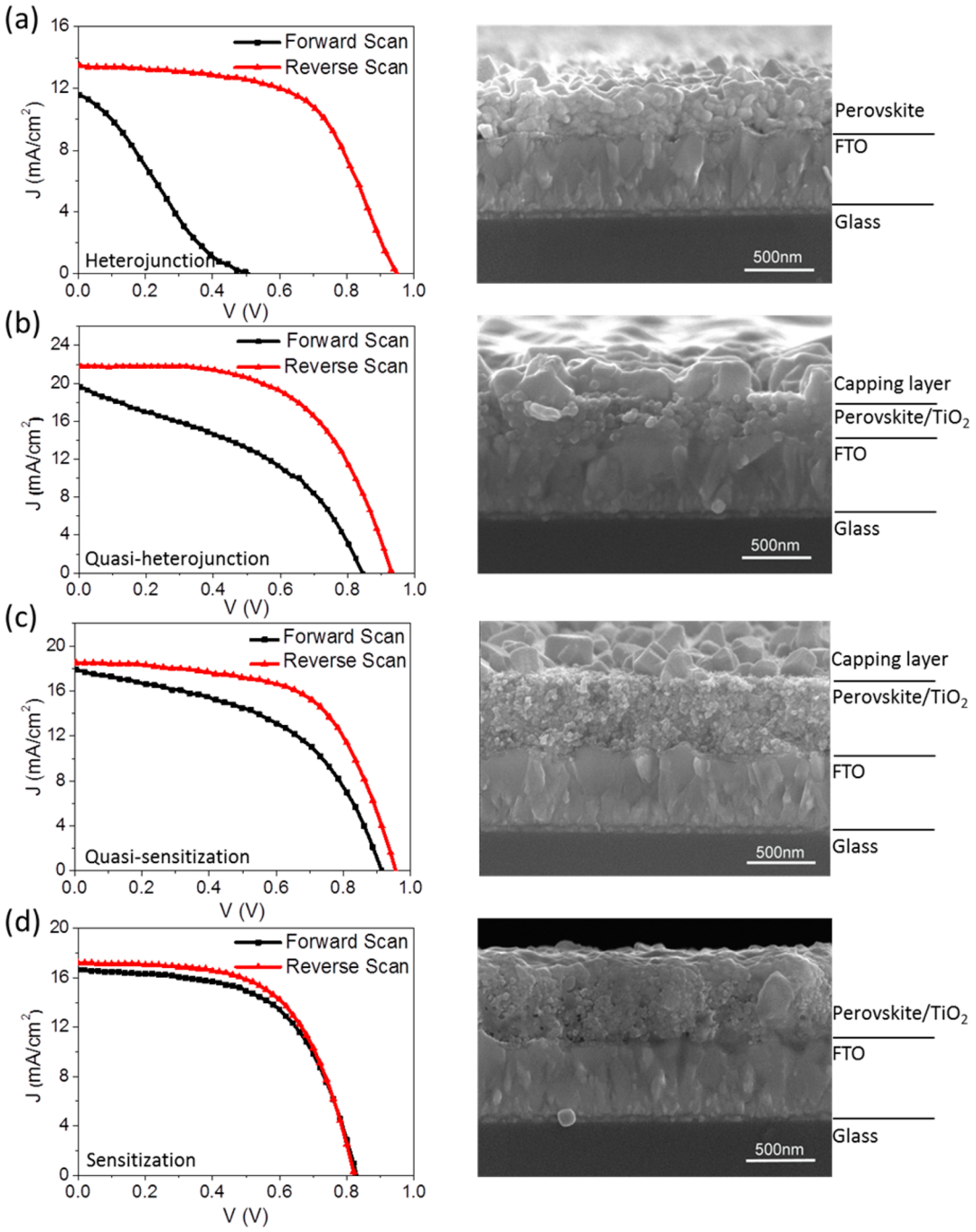

Figure 6. $I-V$ plots and typical SEM images of four types of perovskite solar cells with the architecture changing from heterojunction to sensitization under a scan velocity of 250 mV/s. From (a) to (d), the discrepancy between forward and reverse scan decreases with the TiO_2 scaffold increase, and the perovskite capping layer decreases.

measurement is a better way to evaluate the efficiency of perovskite solar cells.

There are more hysteresis phenomena that can be analyzed by the ferroelectric effect. We found that the hysteresis loop in hybrid perovskite solar cells changes when scanned at different starting points; the efficiency decreases significantly when the scan starts from a more negative bias voltage (Figure 4a,b), which has not been reported before. Different starting points would lead to different initial states of the ferroelectric domain. If a more negative voltage is applied, the initial $E-P$ state will be at the right side of point A in Figure 2a, resulting in an even smaller ε; therefore, the collection efficiency becomes worse assuming the long relaxation time, which influences the $I-V$ hysteresis loop ultimately. For this reason, the forward scan efficiency drops from 5 to 1% when the scan starts from −0.2 and −1 V, respectively (Figure 4a). Note that the inference is not held under higher positive applied voltage, confirmed by our measurements in Figure 4b. Due to the characteristic exponential relation of $I-V$ in the diode, when $V_{app} > V_{open}$, the diode enters into the low resistance area (Figure S3 in the Supporting Information). Therefore, the applied voltage is hard to switch the electrical field (E) across the perovskite material further, which will convert to a large current based on Ohm's Law, $J/E = k$ (conductivity).

dx.doi.org/10.1021/jz502111u | J. Phys. Chem. Lett. 2014, 5, 3937−3945

To give a more comprehensive description of hysteresis in $I-V$ curves of perovskite solar cells, we demonstrate typical $I-V$ curves when solar cells go through a large variation of scanning velocity from 80 to 0.01 V/s (Figure 5). The different hysteresis behaviors in Figure 5 can be explained by three main effects, (i) diffusion capacitance, (ii) junction capacitance, and (iii) ferroelectric capacitance.[6] We suggest that this kind of device will go through three stages considering these three effects when the scan velocity changes from extremely fast to extremely slow. During each stage, different effects contribute to the hysteresis loop due to the different time scale of each effect. From 80 to 20 V/s (Figure 5a,b) (stage I), the efficiency discrepancy ($PCE_{(reverse\ scan)} - PCE_{(forward\ scan)}$) decreases from 1.5 to 0.9%, and we speculate that the polarization state cannot respond in time and almost stays at its initial state during the scan. Caused by the capacitor current $I_c = C^*(dv/dt) \approx 1-2$ mA/cm^2, the loop becomes more obvious under higher scan velocity. From 20 to 10 V/s (stage II), the efficiency discrepancy decreases from 0.9 to 0.5%. In this case, the capacitor effect and the carrier diffusion effect and even the ferroelectric effect might combine to impact the hysteresis loop. From 10 V/s to 250 mV/s (stage III), the efficiency discrepancy increases from 0.6 to 3.2%. The anomalous hysteresis loop is due to the extremely long ferroelectric state relaxation time. Due to the short measure time of about 0.3 s (10 V/s), the domain structure in perovskite can not respond in time, and the polarization remains unchanged in this scan cycle. However, when the scan velocity decreases to a moderate value of 0.25 V/s, the domain structure can be varied when reverse scan begins; therefore, during this scan cycle, the dielectric constant goes through a larger variation in a longer measurement time of 12 s compared to 0.3 s, causing a more obvious hysteresis under slower scan velocity. As shown in the stable-state $I-V$ curves (Figure 3c,f), if the cells are measured under extremely slow velocity of 0.01 V/s (stage IV), the discrepancy will decrease again.

As we know, many groups[4,6,24,26] had already reported that the hysteresis strongly relies on the architecture of solar cells. For instance, planar heterojunction devices exhibit more pronounced hysteresis than mesoporous TiO_2-based devices. However, the underlying reason and physics have not been given. Herein, four different architectures of hybrid perovskite solar cells were fabricated to show that as the thickness of the perovskite capping layer decreases, hysteresis behavior becomes weaker. Figure 6 demonstrates the four types of perovskite solar cells, a heterojunction solar cell without a mesoporous TiO_2 scaffold (type I, Figure 6a), a quasi-heterojunction with a 200 nm scaffold and 200 nm capping layer on it (type II, Figure 6b), quasi-sensitization with a folded thicker scaffold and thinner capping layer (type III, Figure 6c), and a sensitized solar cell with a much thicker scaffold and no capping layer (type IV, Figure 6d). Here, we define a parameter $D = (PCE_{(reverse\ scan)} - PCE_{(forward\ scan)})/PCE_{(reverse\ scan)}$ to evaluate the difference between reverse and forward scan measurements. The D values for these four types of devices are $D1 = 52.2\%$, $D2 = 42.3\%$, $D3 = 25.3\%$, and $D4 = 6.1\%$. In order to confirm the result, 100 devices were fabricated and tested for the four types, and the D value decreased as the solar cell architecture changed from type I to type IV (Figure 7). This indicates that the $I-V$ hysteresis loop gradually disappears when the architecture evolves from a planar heterojunction to perovskite sensitized type by confining more perovskite material into the TiO_2 scaffold, which is very consistent with the previous observations.[9]

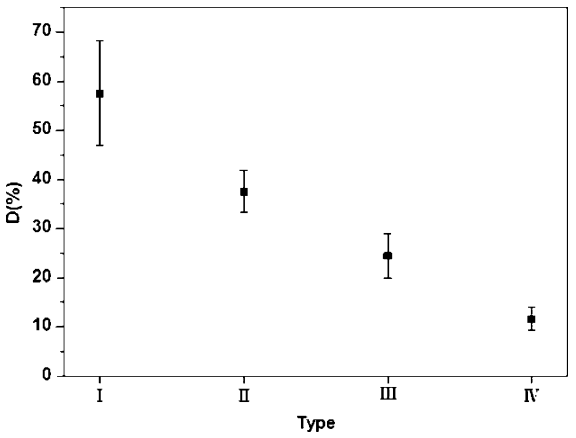

Figure 7. D value of 100 devices for 4 types of perovskite solar cells from the heterojunction (type I) to sensitized (type IV) structure.

The observations can also be explained based on the ferroelectric effect. Considering that the Debye length is constant in ferroelectric material (about 100 nm), one can reduce the number of domain walls when the crystal size becomes smaller than the Debye screening length.[22] When the crystal grain size becomes extremely small (~20 nm), the domain wall, which moves slowly causing the slow process in perovskite, might disappear while the energy band structure in the material is retained. Here, from type I to type IV, when the TiO_2 scaffold becomes thicker, the ratio of perovskite with small grain size increases considering that the perovskite crystal growth is confined by TiO_2; thus, the ferroelectric effect becomes weaker, giving rise to a less pronounced hysteresis behavior. On the other hand, if perovskite particles play a role as a sensitized pigment in the nanostructure scaffold host (type IV), the internal electric field distribution is mainly decided by the TiO_2 scaffold and HTM (hole transporting material) (Figure S4 in the Supporting Information). Thus, the polarization of the perovskite particles has little influence on the photoelectric properties of the solar cells, even if the ferroelectric domain still exists in these nanoparticles.

Although we have explained the observed hysteresis based on the ferroelectric effect in perovskite solar cells, the origin of those ferroelectric domains in this material is not yet clear. Some groups thought that the high rotation rates (ps) of $CH_3NH_3^+$ at room temperature may be the origin, but it is not consistent with the time interval of $I-V$ measurement.[21] It is reported recently that the dipole−dipole interaction could minimize the energy so that the molecular ferroelectric can be formed.[8] We speculate that Pb−I_3 cages can also attribute to the ferroelectric effect in addition to the MA^+ molecules.

Additionally, by exponentially simulating the stable-state curves $I(t)$ (Figure 3), we can find that the relaxation time ranges from 0.1 to 10 s when a different voltage is applied, which is consistent with previous analysis.[7] Why is there such a difference in the relaxation time under different bias voltages? It might be an important issue related to this material and also implies the electric-field-dependent motion of the ferroelectric domain wall, which needs further investigation.

In addition to the ferroelectric effect, some other possibilities have been proposed to contribute to the hysteresis, like defect states and excess ions migration.[6−10] However, these two speculations can infer some results that are different from the experimental observations[6,27−29] (see discussions in the Supporting Information) and maybe need further research.

dx.doi.org/10.1021/jz502111u | J. Phys. Chem. Lett. 2014, 5, 3937−3945

In summary, we demonstrate strong evidence to show that the anomalous hysteresis observed in hybrid perovskite solar cells is caused by the ferroelectric effect. On the basis of its corresponding ferroelectric diode model in solar cells, we carefully analyze the role of this special effect on the solar cells' efficiency from two aspects, excess polarization and nonlinear permittivity. From the long-stepwise measurement results, we confirm the long relaxation time of ∼10 s in hybrid perovskite solar cells with a capping layer. Compared to the actual efficiency obtained from the stable-state value, it is usually over- or underestimated for reverse/forward scan under 0.25 V/s. We suggest the proper measurements to characterize the perovskite solar cells to depress the anomalous hysteresis. We give specific and detailed explanation for these hysteresis phenomena. For a known phenomenon in which a different architecture has different hysteretic behavior, it is related to the domain wall motion, which depends on the grain size of the perovskite. For perspective, the ferroelectric effects strongly affect the performance of the hybrid perovskite solar cells, which needs to be considered in the optimization of perovskite solar cells. The hybrid perovskite paves the way to the investigation of ferroelectric semiconductors in photovoltaic applications.

■ ASSOCIATED CONTENT

Supporting Information

Device fabrication and solar cell characterization details. XRD data of peroskite materials. Scheme of the $E-P$ loop measurement device. Typical $I-V$ curve of a diode. Architecture and corresponding potential distribution for planar-type and sensitized-type perovskite solar cells. Discussion about hysteresis analysis based on defect states and excess ions migration. This material is available free of charge via the Internet at http://pubs.acs.org.

■ AUTHOR INFORMATION

Corresponding Authors

*E-mail: zhaoqing@pku.edu.cn (Q.Z.).
*E-mail: yudp@pku.edu.cn (D.Y.).

Author Contributions

⊥J.W. and Y.Z contributed equally to this work.

Notes

The authors declare no competing financial interest.

■ ACKNOWLEDGMENTS

We thank Prof. Yuan Li for Raman measurement and Prof. Kexin Liu for FTIR measurement. This work was supported by National 973 projects (2011CB707601, 2013CB932602, MOST) from the Ministry of Science and Technology, China and the National Natural Science Foundation of China (NSFC51272007, 11023003, 11234001). Q.Z acknowledges the Beijing Nova Program (XX2013003) and the Program for New Century Excellent Talents in University of China.

■ REFERENCES

(1) Zhou, H.; Chen, Q.; Li, G.; Luo, S.; Song, T. B.; Duan, H. S.; Hong, Z.; You, J.; Liu, Y.; Yang, Y. Interface engineering of highly efficient perovskite solar cells. *Science* **2014**, *345*, 542−546.

(2) O'regan, B.; Grätzel, M. A low-cost, high-efficiency solar cell based on dye-sensitized. *Nature* **1991**, *353*, 737−740.

(3) Burschka, J.; Pellet, N.; Moon, S. J.; Humphry-Baker, R.; Gao, P.; Nazeeruddin, M. K.; Grätzel, M. Sequential deposition as a route to high-performance perovskite-sensitized solar cells. *Nature* **2013**, *499*, 316−319.

(4) Jeon, N. J.; Noh, J. H.; Kim, Y. C.; Yang, W. S.; Ryu, S.; Seok, S. I. Solvent engineering for high-performance inorganic−organic hybrid perovskite solar cells. *Nat. Mater.* **2014**, *13*, 897−903.

(5) Liu, M.; Johnston, M. B.; Snaith, H. J. Efficient planar heterojunction perovskite solar cells by vapour deposition. *Nature* **2013**, *501*, 395−398.

(6) Snaith, H. J.; Abate, A.; Ball, J. M.; Eperon, G. E.; Leijtens, T.; Noel, N. K.; Stranks, S. D.; Wang, J. T. W.; Wojuciechowski, K.; Zhang, W. Anomalous hysteresis in perovskite solar cells. *J. Phys. Chem. Lett.* **2014**, *5*, 1511−1515.

(7) Sanchez, R. S.; Gonzalez-Pedro, V.; Lee, J. W.; Park, N. G.; Kang, Y. S.; Mora-Sero, I.; Bisquert, J. Slow dynamic processes in lead halide perovskite solar cells. Characteristic times and hysteresis. *J. Phys. Chem. Lett.* **2014**, *5*, 2357−2363.

(8) Frost, J. M.; Butler, K. T.; Walsh, A. Molecular ferroelectric contributions to anomalous hysteresis in hybrid perovskite solar cells. *APL Mater.* **2014**, *2*, 081506.

(9) Kim, H. S.; Park, N. G. Parameters affecting $I-V$ hysteresis of $CH_3NH_3PbI_3$ perovskite solar cells: Effects of perovskite crystal size and mesoporous TiO_2 layer. *J. Phys. Chem. Lett.* **2014**, *5*, 2927−2934.

(10) Frost, J. M.; Butler, K. T.; Brivio, F.; Hendon, C. H.; van Schilfgaarde, M.; Walsh, A. Atomistic origins of high-performance in hybrid halide perovskite solar cells. *Nano Lett.* **2014**, *14*, 2584−2590.

(11) Noblanc, O.; Gaucher, P.; Calvarin, G. Structural and dielectric studies of Pb $(Mg_{1/3}Nb_{2/3})$ O_3−$PbTiO_3$ ferroelectric solid solutions around the morphotropic boundary. *J. Appl. Phys.* **1996**, *79*, 4291−4297.

(12) Tohge, N.; Takahashi, S.; Minami, T. Preparation of $PbZrO_3$−$PbTiO_3$ ferroelectric thin films by the sol−gel process. *J. Am. Ceram. Soc.* **1991**, *74*, 67−71.

(13) Wang, H.; Wang, C. H.; Li, G.; Jin, T.; Liao, F.; Lin, J. Synthesis, structure, and characterization of the series $BaBi_{1-x}Ta_xO_3$ $(0 \le x \le 0.5)$. *Inorg. Chem.* **2010**, *49*, 5262−5270.

(14) Frey, M. H.; Payne, D. A. Grain-size effect on structure and phase transformations for barium titanate. *Phys. Rev. B* **1996**, *54*, 3158−3168.

(15) Rysiakiewicz, P. E.; Poprawski, R.; Urbanowicz, A.; Maczka, M. Porous glasses with sodium nitrite impregnations. *Opt. Appl.* **2005**, *35*, 769−774.

(16) Sugai, S. Dimerization model for the metal−semiconductor transition in $BaPb_{1-x}Bi_xO_3$. *Phys. Rev. B* **1987**, *35*, 3621.

(17) Poglitsch, A.; Weber, D. Dynamic disorder in methylammonium trihalogenoplumbates (II) observed by millimeter-wave spectroscopy. *J. Chem. Phys.* **1987**, *87*, 6373−6378.

(18) Baikie, T.; Fang, Y.; Kadro, J. M.; Schreyer, M.; Wei, F.; Mhaisalkar, S. G.; Grätzel, M.; White, T. J. Synthesis and crystal chemistry of the hybrid perovskite (CH_3NH_3) PbI_3 for solid-state sensitised solar cell applications. *J. Mater. Chem. A* **2013**, *1*, 5628−5641.

(19) Quarti, C.; Grancini, G.; Mosconi, E.; Bruno, P.; Ball, J. M.; Lee, M. M.; Snaith, H. J.; Petrozza, A.; Angelis, F. D. The Raman spectrum of the $CH_3NH_3PbI_3$ hybrid perovskite: Interplay of theory and experiment. *J. Phys. Chem. Lett.* **2014**, 279−284.

(20) Mosconi, E.; Quarti, C.; Ivanovska, T.; Ruani, G.; De Angelis, F. Structural and electronic properties of organo-halide lead perovskites: A combined IR-spectroscopy and ab initio molecular dynamics investigation. *Phys. Chem. Chem. Phys.* **2014**, *16*, 16137−16144.

(21) Stoumpos, C. C.; Malliakas, C. D.; Kanatzidis, M. G. Semiconducting tin and lead iodide perovskites with organic cations: Phase transitions, high mobilities, and near-infrared photoluminescent properties. *Inorg. Chem.* **2013**, *52*, 9019−9038.

(22) Strukov, B. A.; Levanyuk, A. P. *Ferroelectric phenomena in crystals: physical foundations*; Springer: New York, 1998; Vol. *5*, pp 201−206.

(23) Blom, P. W. M.; Wolf, R. M.; Cillessen, J. F. M.; Krijn, M. P. C. M. Ferroelectric schottky diode. *Phys. Rev. Lett.* **1994**, *73*, 2107.

(24) Grätzel, M. The light and shade of perovskite solar cells. *Nat. Mater.* **2014**, *13*, 838−842.

(25) Gao, P.; Britson, J.; Jokisaari, J. R.; Nelson, C. T.; Baek, S. H.; Wang, Y.; Eom, C. B.; Chen, L. Q.; Pan, X. Atomic-scale mechanisms of ferroelastic domain-wall-mediated ferroelectric switching. *Nat. Commun.* **2013**, *4*, 2791.
(26) Ku, Z.; Rong, Y.; Xu, M.; Liu, T.; Han, H. Full printable processed mesoscopic $CH_3NH_3PbI_3/TiO_2$ heterojunction solar cells with carbon counter electrode. *Sci. Rep.* **2013**, *3*, 3132.
(27) Kim, J.; Lee, S. H.; Lee, J. H.; Hong, K. H. The role of intrinsic defects in methylammonium lead iodide perovskite. *J. Phys. Chem. Lett.* **2014**, *5*, 1312−1317.
(28) Leijtens, T.; Stranks, S. D.; Eperon, G. E.; Lindblad, R.; Johansson, E. M.; McPherson, I. J.; Rensmo, H.; Ball, J. M.; Lee, M. M.; Snaith, H. J. Electronic properties of meso-superstructured and planar organometal halide perovskite films: Charge trapping, photodoping, and carrier mobility. *ACS Nano* **2014**, *8*, 7147−7155.
(29) Mei, A.; Li, X.; Liu, L.; Ku, Z.; Liu, T.; Rong, Y.; Xu, M.; Hu, M.; Chen, J.; Yang, Y.; et al. A hole−conductor-free, fully printable mesoscopic perovskite solar cell with high stability. *Science* **2014**, *345*, 295−298.